Primerjava količine TEC (vsebnost elektronov v stolpcu zraka) nad Evropo v letih sončnega minimuma in maksimuma (2020 in 2024)

Comparison of Total Electron Content Sources Over Europe During Solar Minimum and Maximum Years (2020 and 2024)

Stefan Krstić, Miljana Todorović-Drakul, Sanja Grekulović, Dušan Petković, Oleg Odalović

UDK: 537.533.8(4)
Klasifikacija prispevka po COBISS.SI: 1.01
Prispelo: 21. 2. 2025
Sprejeto: 10. 9. 2025

DOI: 10.15292/geodetski-vestnik.2025.04.574-593
SCIENTIFIC ARTICLE
Received: 21. 2. 2025
Accepted: 10. 9. 2025

IZVLEČEK

V članku smo predstavili primerjavo količine TEC (total electron content oziroma vsebnost elektronov v stolpcu zraka), pridobljene iz različnih virov: ionosond, modela IRI, modela NeQuick in globalnih navigacijskih satelitskih sistemov (GNSS). Študija je bila izvedena na več lokacijah, enakomerno razporejenih po vsej Evropi. Za leti 2020 in 2024 smo analizirali vrednosti TEC iz navedenih virov, in sicer za šest dni v letu. V raziskavi smo ugotovili, da ionosonde na splošno proizvajajo najmanjše vrednosti TEC. Podatki GNSS zagotavljajo TEC z najvišjimi vrednostmi v mirnih obdobjih, medtem ko model NeQuick ustvari najvišje vrednosti, ko se Sončeva in geomagnetna aktivnost povečata. Primerjava korelacijskega koeficienta dnevnih sprememb TEC iz različnih virov kaže na veliko podobnost. Glede na pridobljene vrednosti RMS iz razlik v TEC smo ugotovili, da več virov TEC daje vrednosti z zadovoljivo stopnjo skladnosti po vsej Evropi. Skladnost je okrog nekaj enot TECU v solarnem minimumu in znotraj 10 enot TECU v solarnem maksimumu. TEC iz modelov IRI in NeQuick sta zelo skladna v obeh Sončevih obdobjih. V obdobju solarnega minimuma so nekoliko večja odstopanja med TEC iz ionosond in tistimi iz modela NeQuick ter GNSS, medtem ko druge razlike ostajajo majhne. V obdobju solarnega maksimuma ionosonde in model NeQuick kažejo največje razlike in variacije.

KLJUČNE BESEDE

vsebnost elektronov v stolpcu zraka (TEC), GNSS, IRI, NeQuick, iosonda

ABSTRACT

In this paper, we present a comparison of Total Electron Content (TEC) obtained from various sources: ionosondes, the IRI model, the NeQuick model, and Global Navigation Satellite Systems (GNSS). The study was conducted at multiple locations distributed evenly throughout Europe. We analyzed TEC values from the aforementioned sources during six days per year for 2020 and 2024. In our research, we found that ionosondes generally yield the lowest estimated TEC values. GNSS data provide TEC with the highest values during quiet periods, while the NeQuick model generates the highest values when solar and geomagnetic activity increases. Based on the correlation coefficient, diurnal variations in TEC from different sources showed significant similarities. Focusing on RMS (root mean square) values of TEC differences, we discovered that several TEC sources produce TEC with a satisfactory level of consistency across Europe. Consistency is several TECU during the solar minimum and within 10 TECU during the solar maximum. TEC from the IRI and NeQuick models is highly consistent at both solar periods. During the solar minimum period, there are slightly larger discrepancies between TEC from ionosondes and those from the NeQuick model and GNSS, while other differences stay small. During the solar maximum period, ionosondes and the NeQuick model show the largest differences and variations.

KEY WORDS

Total Electron Content (TEC), GNSS, IRI, NeQuick, ionosonde

1 INTRODUCTION

The ionosphere is a part of Earth's atmosphere that begins approximately 50 km above the Earth's surface and extends beyond 1000 km. The ionospheric layer is distinguished by a significant concentration of free electrons and ions, formed through the ionization of neutral particles by intense ultraviolet radiation from the Sun and by collisions with energetic particles that penetrate the atmosphere (Schunk & Nagy, 2009). The ionosphere is categorized into several layers based on electron density distribution with altitude: D (50–90 km), E (90–140 km), and F (above 140 km). The F layer splits into the regions F1 (140–200 km) and F2 (200–1000 km) during the day. The maximum electron density can be found in the F2 layer, whereas the D layer contains a much smaller number of free electrons (Xu et al., 2021).

The ionosphere causes one of the largest errors in positioning using Global Navigation Satellite Systems (GNSS) (Hoque & Jakowski, 2008). For the radio waves that are used within GNSS technology, the ionosphere is a dispersive medium. The ionosphere's impact on GNSS signals and other electromagnetic waves mostly depends on the number of free electrons present in it (Klobuchar, 1991). The factor that represents its quantity at a certain location is the Total Electron Content (TEC). The TEC is influenced by the solar activity, diurnal and seasonal variations, and the Earth's magnetic field (Hofmann-Wellenhof et al., 2008). We use the acronym VTEC (vertical TEC) to emphasize that it pertains to the zenith direction (Hernández-Pajares et al., 2009). TEC is generally expressed in TEC Units (TECU), where 1 TECU = 10^{16} electrons per m^2. Determining TEC and developing ionospheric models can greatly enhance the accuracy of single-frequency positioning techniques by mitigating ionospheric delay.

Various instruments can be used to determine TEC at a specific location. Ionosondes, as instruments for researching the ionosphere, are among them (Klipp et al., 2020). Along with that, we analyzed TEC values derived from GNSS measurements (Ciraolo et al., 2007; Seemala, 2023). The complexity of the ionosphere has led to several methodologies for its modeling. To attain simplicity, some of the models have been restricted to specific altitude or latitude ranges, while others have been restricted to certain ionospheric parameters, such as TEC (Memarzadeh, 2009). Various ionospheric models represent the ionosphere based on diverse data sets. Certain data sets have been collected using the previously mentioned equipment; however, additional data have been applied. We used the IRI (Bilitza et al., 2022) and NeQuick (Nava et al., 2008) models to compute TEC values.

Many researchers (Ameen et al., 2019; Atıcı, 2018; Chen et al., 2020; Guo et al., 2021; Kayode et al., 2024; Odeyemi et al., 2018; Yasyukevich et al., 2023) have studied and evaluated the performance of various TEC sources across numerous geographical locations and under different circumstances. Here, we compared TEC sources across several European sites through the years 2020 and 2024. The study by Todorović Drakul et al. (2021) examines TEC values from the IRI and NeQuick models and compares them with values from GNSS measurements over the Balkan Peninsula in 2019 during periods of higher solar . The TEC values derived from the IRI and NeQuick models showed discrepancies from GNSS TEC values for several TECU.

In this study, we used the following TEC sources: ionosonde, IRI model, NeQuick model, and GNSS observations. We analyzed and compared TEC values from the mentioned sources at six locations spread across Europe (one location each in Norway, the United Kingdom, the Czech Republic, Italy, Greece, and Spain). The analysis performed focuses on the years 2020 and 2024. The year 2020 marks the beginning

of the 25th solar cycle, characterized by the solar minimum phase. Conversely, the year 2024 is significant because it is close to the solar maximum phase of the 25th solar cycle. We selected the equinoxes and solstices of both years as occasions when the Sun and Earth significantly change their relative positions. In addition, we identified two additional days in each of these years characterized by interesting solar and geomagnetic conditions. In 2020, we chose two days characterized by minimal solar and geomagnetic activity, while in 2024, we selected two days marked by extremely high solar and geomagnetic activity. In our research, we examined the absolute TEC levels of each source and their temporal variations. We identified noteworthy trends in absolute TEC levels from different sources. Initially, we created differences among each TEC source at all specified locations and dates for purposes of comparison. We calculated several statistical parameters to analyze the TEC differences based on the data. By focusing on the root mean square (RMS) of the resulting TEC discrepancies, we reached conclusions regarding the matching of TEC values between each pair of sources. From the obtained average RMS values and their deviations, we also gained insight into the magnitude of the differences and their consistency.

2 TEC SOURCES ANALYZED

Since this paper compares the values of vertical TEC derived by applying ionosonde, GNSS technology, the IRI model, and the NeQuick model, the individual sources of TEC used in the work will be briefly described below.

2.1 Application of Ionosonde

An ionosonde, or ionospheric sounder, is a radar device intended to study the Earth's ionosphere, with its development commencing in the 1920s. Modern digital ionosondes (digisondes) are used to gather high-resolution data on the ionosphere, enabling real-time monitoring of ionospheric conditions. These instruments use high-frequency (HF) radio waves. The ionosonde operates by emitting short radio pulses of varied frequencies vertically. The generated pulses travel to the ionosphere, where its layers reflect them. We then monitor the return signals to determine these layers' virtual heights based on the radio waves' travel time (Schunk & Nagy, 2009).

Data from the ionosonde generates an ionogram, a graph that shows the virtual height of the ionosphere as a function of frequency, allowing for the assessment of the Earth's ionospheric state and the alterations occurring within it. The ionogram may be analyzed either manually or automatically using suitable software. The ionogram allows for the derivation of the vertical profile of electron density. The TEC above the ionosonde is calculated by integrating the acquired electron density concerning altitude (Klipp et al., 2020).

The Global Ionospheric Radio Observatory (GIRO) provides data collected by ionosondes. GIRO is a multinational project whose goal is to collect and distribute data on the ionosphere obtained by sondes using HF signals, which are distributed around the world (Galkin & Reinisch, 2011). GIRO includes three main components (Reinisch & Galkin, 2011):

1. The network of ionosondes,
2. Two main databases (DIDBase and DriftBase), and
3. Software that enables automated data analysis and generates advanced outputs for end users.

For the purposes of this work, GIRO services were used to automatically obtain TEC from ionograms stored in the DIDBase (Digital Ionogram Data Base). Services that derive the relevant data from the ionogram can be accessed using the web address https://giro.uml.edu/didbase/scaled.php.

2.2 Application of GNSS Technology

The ionosphere significantly impacts positioning via GNSS technology (Hofmann-Wellenhof et al., 2008). Therefore, for precise positioning, it is necessary to model the ionospheric influence (Memarzadeh, 2009). However, by applying the inverse approach, it is possible to determine the influence of the ionosphere on the signals emitted by the GNSS satellites using GNSS observations. Since the influence of the ionosphere on GNSS signals primarily depends on the TEC, determining this influence allows the estimation of the unknown TEC. On this occasion, the dispersiveness of the ionosphere is used as the medium of propagation of electromagnetic waves. Due to the dispersive nature of the ionosphere, ionospheric influences on GNSS signals depend on the value of their frequencies.

GNSS technology determines pseudoranges by measuring the time signal from the satellite to the receiver through code and phase measurements. The ionosphere causes a time delay in the signal emitted at frequency *f*, given by the formula (Cooper et al., 2019; Davies, 1990; Hargreaves, 1992; Sardón et al., 1994):

$$\delta t = \frac{40.3}{c \cdot f^2} TEC, \tag{1}$$

where *c* is the speed of light in the vacuum, while constant 40.3 is expressed in units $\frac{m^3}{s^2}$.

Using GNSS observations at two frequencies (f_1 and f_2) and utilizing the dispersiveness of the ionosphere, we derive a formula for the TEC as a function of the differences in signal time delays ($\Delta t = \delta t_2 - \delta t_1$):

$$TEC = \frac{c \cdot \Delta t}{40.3} \cdot \frac{f_1^2 \cdot f_2^2}{f_1^2 - f_2^2}. \tag{2}$$

Both code and phase GNSS measurements are used to determine signal time delay differences in an unambiguous and precise way. In this method of estimating TEC, corrections for Differential Code Biases (DCB) are applied to eliminate the influence of hardware delays of satellite and receiver signals (more in (Ciraolo et al., 2007; Dach et al., 2015; Memarzadeh, 2009)).

The TEC obtained using this technique is slant TEC (STEC); however, by applying the suitable mapping function *F*(*z*), which depends on the satellite zenith angle, we can determine VTEC (Foelsche & Kirchengast, 2002; J. Klobuchar, 1987; Schaer, 1999; Wu et al., 2021; Xiang & Gao, 2019):

$$VTEC = \frac{STEC}{F(z)}. \tag{3}$$

In this approach, the most common model is the single-layer ionosphere at a height of 350 km.

To determine the TEC values, the GNSS data were processed using the *GPS-TEC analysis* software developed by Gopi Seemala (currently employed at the Indian Institute of Geomagnetism). The software was downloaded in its latest version, 3.5, from the website https://seemala.blogspot.com/. This

software is reliable, accessible, and aligned with widely accepted ionospheric data processing standards. The algorithm employed in the development of this program is described in (Seemala, 2023). This reference provides comprehensive information regarding the procedure of deriving TEC from raw GNSS measurements. It also explains how to handle and apply DCB corrections for both satellites and receivers and how to convert slant TEC to vertical TEC using the thin-shell model and the related geometric mapping function. Other key processing steps, such as elevation angle filtering and data formatting, are also fully documented in the same source.

2.3 IRI Model

The IRI model is being developed as a standard ionosphere model as part of the International Reference Ionosphere (IRI) project. The Committee on Space Research (COSPAR) and the International Union of Radio Science (URSI) provide the IRI working group for its development. The IRI model is recognized as the official standard for the Earth's ionosphere by the International Organization for Standardization (ISO), the International Union of Radio Science, the Committee on Space Research, and the European Cooperation for Space Standardization, leading to its wide application in science, engineering, and education. This is an empirical (data-based) model that provides the main ionospheric parameters based on a long history of observations of the ionosphere from both space and the ground (Bilitza et al., 2022).

The IRI model is continuously developed and improved yearly, utilizing many global data sources, including information from ionosondes, terrestrial radar systems, and satellites. The current version is IRI-2020. The reliability of the IRI as an empirical model depends on the spatial and temporal coverage of the underlying datasets. A high data availability at mid latitudes ensures good accuracy; however, performance degrades in places at high and low latitudes when data availability is not comparable to that at mid latitudes. The Northern Hemisphere has a far denser network of stations, which impacts model accuracy. The development of the IRI model is described in detail in the report (Bilitza, 1990), while (Bilitza et al., 2022) discuss the most recent version of the model. A compilation of special publications presenting progress in the IRI model development process is available at https://irimodel.org/docs/asr_list.html.

The results used in this work represented as TEC derived from the IRI model were provided by the Community Coordinated Modelling Center (CCMC) at the Goddard Space Flight Center through their publicly available services (https://ccmc.gsfc.nasa.gov). The IRI-2020 model, created by the IRI working group, was applied.

2.4 NeQuick Model

The NeQuick model of electron density in the ionosphere is under development at the Telecommunications/ICT for Development (T/ICT4D) Laboratory of the Abdus Salam International Centre for Theoretical Physics (ICTP) in Trieste, Italy, in collaboration with the Institute of Geophysics, Astrophysics and Meteorology at the University of Graz, Austria. The European Space Agency has adopted the first version of the model for assessment analysis and single-frequency positioning applications within the European Galileo project. The International Telecommunication Union, Radiocommunication Sector

also acknowledged it as a suitable method for TEC modeling. Similar to the IRI model, the NeQuick model combines several data sources to represent the ionosphere's conditions, such as data from ionosondes, radar systems, and satellite missions. As in the case of other models, numerous efforts are being made to enhance the NeQuick analytical formulation, leveraging the increasing amount of available data, resulting in constant updates to NeQuick. The present version of the model is NeQuick 2, as detailed in (Nava et al., 2008).

To calculate the TEC values using the NeQuick 2 model, publicly accessible services from the website https://t-ict4d.ictp.it/nequick2 were applied. The NeQuick provides electron density for locations in the ionosphere, utilizing height, geocentric latitude, and geocentric longitude as coordinates on a spherical Earth. The model values are contingent upon solar activity, season, and time. The NeQuick model contains algorithms for evaluating the electron density along any straight ground-to-satellite ray path and corresponding TEC by numerical integration.

3 METHODOLOGY

We analyzed the vertical TEC values during the solar minimum and solar maximum of the 25th solar cycle. The representatives for the solar minimum period encompassed the equinoxes and solstices of 2020, the year that commenced the 25th solar cycle, along with two additional days chosen for their exceptionally low solar and geomagnetic activity (14/05/2020 and 10/07/2020). The representations for the solar maximum period included the equinoxes and solstices of 2024, in addition to two extra days chosen for their extremely high solar and geomagnetic activity (11/5/2024 and 03/10/2024). This is summarized in Table 1, which contains the following indicators that quantify the mentioned activity (Matzka et al., 2021):

- International Sunspot Number (SN),
- F10.7 Solar Radio Flux, and
- Daily equivalent Planetary Amplitude A_p.

Table 1: Indicators of solar and geomagnetic activity (taken from https://kp.gfz-potsdam.de/en/data)

Date	SN	F10.7	A_p
20/03/2020	0	71.7	6
14/05/2020	0	69.0	2
20/06/2020	0	67.8	5
10/07/2020	0	71.1	2
22/09/2020	0	72.4	5
21/12/2020	12	79.6	12
20/03/2024	123	174.1	4
11/05/2024	173	218.0	271
20/06/2024	165	210.0	6
22/09/2024	129	164.0	5
03/10/2024	207	312.1	7
21/12/2024	164	194.7	14

Besides the solar and geomagnetic activity indicators presented in the previous table, it is essential to

point out solar X-ray flares on selected additional days in 2024. On 11/5/2024, two X-ray flares were recorded, one of which was very strong, classified as X5.89. On 03/10/2024, a powerful X-ray flare designated as X9.05 occurred (according to https://www.spaceweatherlive.com).

3.1 Data Description

Six locations were chosen to compare the TEC values obtained from different sources, covering the area of Europe reasonably well (Figure 1). We compared the vertical TEC at these sites, which were derived from the described sources. We chose each location to ensure the presence of both an ionosonde and a GNSS station nearby, enabling the collection of all necessary data.

GIRO services were applied to ionosondes designated by their locations to acquire vertical TEC from ionogram data. The corresponding VTEC from other sources refers to mutually identical positions that maximally differ from the ionosondes by 0.6° in latitude (φ) and 0.8° in longitude (λ) (Table 2). We processed GNSS data downloaded from the EPN (EUREF Permanent Network) using the *GPS-TEC analysis* program to determine the vertical TEC values. The data were downloaded from the corresponding GNSS stations (Table 2) in RINEX format (Receiver Independent Exchange format).

Since IRI and NeQuick are ionospheric models, they allow greater flexibility in the choice of locations. Using the IRI model, different ionospheric parameters can be determined for an arbitrarily given position and time. The NeQuick model can assess electron density and associated TEC for any straight pathway above Earth. We calculated the vertical TEC values using the IRI and NeQuick models at the same locations utilized by the GNSS approach (Table 2), applying the appropriate services. To compute VTEC values based on the IRI model, we used the default parameters at https://kauai.ccmc.gsfc.nasa.gov/instantrun/iri/. The determination of TEC employing the NeQuick model was conducted through the NeQuick 2 Web model (https://t-ict4d.ictp.it/nequick2/nequick-2-web-model). We used identical latitudes and longitudes for the endpoints to obtain vertical TEC values. Regarding heights, we made use of electrons within the range of 50 km to 2000 km, consistent with the IRI model.

Table 2: Geographic coordinates of the analyzed locations

Location	Ionosonde		GNSS technology / IRI model / NeQuick model		
	φ [°N]	λ [°E]	Station	φ [°N]	λ [°E]
TROMSO	69.6	19.2	TRO100NOR	69.7	18.9
CHILTON	51.5	359.4	CHIO00GBR	51.1	358.6
PRUHONICE	50.0	14.6	GOPE00CZE	49.9	14.8
ROME	41.9	12.5	M0SE00ITA	41.9	12.5
ATHENS	38.0	23.5	DYNG00GRC	38.1	23.9
EL ARENOSILLO	37.1	353.3	SFER00ESP	36.5	353.8

Figure 1: Spatial distribution of the analyzed locations

The vertical TEC values obtained from all four sources were analyzed hourly, from 00:00 to 23:00 UTC (Coordinated Universal Time), on the designated days in 2020 and 2024 (Table 1). These values were used to conduct a comparative analysis of TEC behavior under varying seasonal and solar activity conditions. TEC values, however, could not be obtained from some sources on particular dates and locations depending on occasional limitations in data availability. In such cases, only those TEC sources with valid data were included in the analysis for the corresponding periods, while unavailable sources were excluded from the direct comparison. A summary of the missing data is presented in Table 3, which highlights the specific gaps for each TEC source and location.

The IRI and NeQuick models provided all the data. TEC from GNSS data was not obtained on several days at three different locations due to the absence of the RINEX files with observation data. The majority of the missing data pertained to results from ionosondes. The GIRO service application failed to provide the TEC to each location for at least a single day. Moreover, it is important to mention that at the CHILTON and ROME locations, we did not obtain TEC data for all selected days in 2024. Due to the lack of data during the solar maximum period, the comparative analysis at these sites was performed just for the remaining TEC sources, excluding ionosondes. In other cases, TEC was successfully obtained for most of the day, with values missing at certain hours.. To ensure meaningful comparisons, TEC values were analyzed only among those sources that provided data for the respective time intervals, and full multi-source comparisons were conducted exclusively for periods with complete data availability.

Table 3: Data availability gaps (ION stands for ionosonde)

TEC Source	Location					
	TROMSO	CHILTON	PRUHONICE	ROME	ATHENS	EL ARENOSILLO
ION	11/05/2024	10/07/2020	10/07/2020	20/03/2024	20/03/2020	20/03/2020
		20/03/2024	11/05/2024	11/05/2024	11/05/2024	14/05/2020
		11/05/2024		20/06/2024		
		20/06/2024		22/09/2024		
		22/09/2024		03/10/2024		
		03/10/2024		21/12/2024		
		21/12/2024				
GNSS					21/12/2020	
				10/07/2020	11/05/2024	20/06/2024
					20/06/2024	

3.2 Parameters for Statistical Analysis of TEC Differences

In accordance with standard statistical analysis literature (Mood et al., 1974; Wilks, 2006), in this study we concentrate on descriptive statistical tools, particularly the root mean square of TEC differences and correlation coefficients, which are especially suited for discovering consistency and agreement between different TEC sources across temporal and spatial domains.

We first evaluated daily consistency of TEC estimates derived from several sources based on hourly TEC values. This evaluation included the comparison of the absolute TEC values with their temporal variations across sources. We calculated the daily correlation coefficient (COR) using the following formula to measure the degree of agreement and the temporal behavior similarity between several TEC sources:

$$COR_{i-j} = \frac{\sum_{k=1}^{n}\left[\left(TEC_{i,k} - \overline{TEC_i}\right)\cdot\left(TEC_{j,k} - \overline{TEC_j}\right)\right]}{\sqrt{\sum_{k=1}^{n}\left(TEC_{i,k} - \overline{TEC_i}\right)^2 \cdot \sum_{k=1}^{n}\left(TEC_{j,k} - \overline{TEC_j}\right)^2}}. \quad (4)$$

Here, i and j refer to different TEC sources: *ION* for ionosonde's measurements, *GNSS* for GNSS measurements, *IRI* for the IRI model, or *NeQ* for the NeQuick model; the index k denotes the hourly epoch within a given day, and n is the number of available hourly TEC values for that day. $TEC_{i,k}$ and $TEC_{j,k}$ represent the TEC values from sources i and j at hour k, while $\overline{TEC_i}$ and $\overline{TEC_j}$ denote the corresponding daily mean TEC values for those sources.

Using the daily COR_{i-j} values, we calculated the mean station-level correlation coefficients $\overline{COR}_{i-j}$ for each location and each pair of TEC source. In addition, we estimated the standard deviations (*SD*) to quantify the variability in daily correlation behavior, using the following formula:

$$SD = \sqrt{\frac{1}{n-1}\sum_{k=1}^{n}((COR_{i-j})_k - \overline{COR}_{i-j})^2}, \quad (5)$$

where $\overline{COR}_{i-j}$ represents the mean of daily correlation values $(COR_{i-j})_k$ at a given location, and n denotes the number of available daily values, which varied between 2 and 6 depending on data availability.

To obtain the overall correlation behaviour across Europe, we computed the average of the station-level $\overline{COR}_{i-j}$ values for each year (2020 and 2024). Corresponding standard deviations were also calculated using the same formulation defined in Equation (5), thereby reflecting the spatial variability of inter-source agreement over the study domain.

Every hour at each selected location, we directly compared the vertical TEC values for each of the chosen days. We formulated the differences between the TEC values obtained from different sources as follows:

$$\Delta TEC_{i-j} = TEC_i - TEC_j, \tag{6}$$

where i and j are different TEC sources. The differences were computed for each hour of the day, considering only the time epochs for which data from both sources (i and j) were simultaneously available. This ensured that the comparison was based solely on matching data points, thereby avoiding bias due to missing values.

Using hourly created differences, we determined certain daily statistical parameters of every ΔTEC_{i-j} for every chosen location: minimum value (*MIN*), maximum value (*MAX*), average (*AVG*), and root mean square (*RMS*). We primarily used the *RMS* parameter for our analysis, as it completely represents TEC differences:

$$RMS_{i-j} = \sqrt{\frac{1}{n}\sum_{k=1}^{n}(\Delta TEC_{i-j})_k^{\,2}}, \tag{7}$$

where n represents the number of hourly TEC differences included in the calculation of daily *RMS*.

We computed the mean values ($\overline{RMS}_{i-j}$) for each location by utilizing the daily RMS_{i-j} values obtained. Additionally, we computed the standard deviation of daily *RMS* values at each location applying the identical approach defined by Equation (5), substituting *COR* values for *RMS* values. Identical to correlation coefficients, we calculated overall averages for each pair of sources, determined as the mean of the stations' averages $\overline{RMS}_{i-j}$ and corresponding standard deviations. To comprehensively assess the differences between TEC sources, we focused on the overall mean RMS values, as they provide a robust single-metric indicator of overall disagreement that is sensitive to both systematic and random deviations.

4 RESULTS

TEC (VTEC) values at EL ARENOSILLO ($\varphi \approx 37°$N), PRUHONICE ($\varphi \approx 50°$N) and TROMSO ($\varphi \approx 70°$N) on days characterized by minimal solar and geomagnetic activity (14/05/2020 and 10/07/2020) and days distinguished by extremely high solar and geomagnetic activity (11/05/2024 and 03/10/2024) are shown in the diagrams presented in Figure 2. The scenarios at the other three locations and on the remaining days are similar.

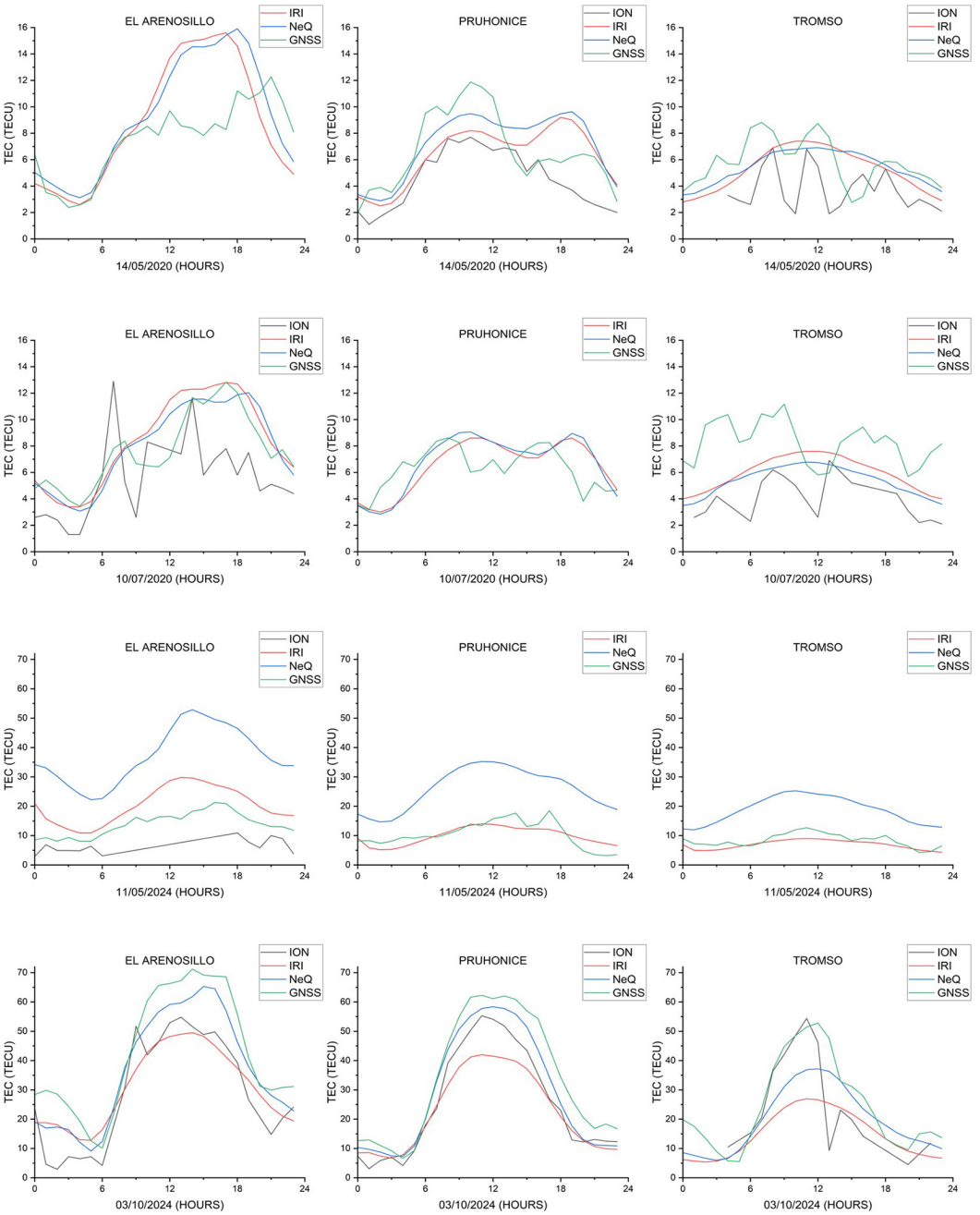

Figure 2: TEC values at locations TROMSO, PRUHONICE, and EL ARENOSILLO during the days 14/05/2020, 10/07/2020, 11/05/2024, and 03/10/2024

Analyzing daily TEC values, we can notice the following:

– All TEC sources produce TEC with the very similar temporal variations.

- The TEC obtained from ionosondes and GNSS data shows rapid temporal variations, while the IRI and NeQuick models yield significantly more gradual variations in outcomes. This distinction is understandable, as the IRI and NeQuick models produce modeled TEC values, but the TEC derived from ionosondes and GNSS represents an empirical estimate based on actual measurements.
- TEC from ionosondes typically exhibits the smallest values under every circumstance.
- The TEC derived from GNSS often stands out with the highest values, particularly during the solar minimum period; yet, increased solar and geomagnetic activity corresponds with greater TEC from the NeQuick (21/12/2020).
- During the solar maximum period, the NeQuick model's TEC usually shows the highest values. Intense geomagnetic activity aligns with markedly elevated TEC values from the NeQuick model (11/05/2024).
- The IRI model provides TEC values that closely align with those of the NeQuick model, especially during the solar minimum phase. In general, the IRI model yields TEC values slightly lower than those from the NeQuick model; however, on 22/09/2024, the situation is reversed, with the IRI model generating TEC values slightly higher than NeQuick. This day is distinguished as a day within the solar maximum period, which has decreased solar and geomagnetic activity.

5 DISCUSSION

We begin the discussion by analyzing the correlation coefficients between different TEC sources. As both the solar minimum (Table 4) and solar maximum (Table 5) periods showed a high level of correlation among TEC sources, no significant variations were noted between them. Along with a very low standard deviation (0.01), the IRI and NeQuick models consistently produced the highest correlation (0.98), so indicating great agreement between these two models in both periods. The remaining correlation coefficients generally had standard deviations of 0.16 and ranged from 0.74 to 0.79 throughout the solar minimum period. It is important to highlight that at TROMSO, the northernmost station in our dataset, we observed significantly lower correlations and larger variations, particularly when GNSS was one of the sources, suggesting increased divergence in source agreement at higher latitudes under low solar activity conditions.

Table 4: The average COR values at all locations and their respective average values in 2020

Location	$\overline{COR}_{ION\text{-}IRI}$	$\overline{COR}_{ION\text{-}NeQ}$	$\overline{COR}_{ION\text{-}GNSS}$	$\overline{COR}_{IRI\text{-}NeQ}$	$\overline{COR}_{IRI\text{-}GNSS}$	$\overline{COR}_{NeQ\text{-}GNSS}$
TROMSO	0.68	0.68	0.53	0.99	0.46	0.47
SD	0.19	0.19	0.20	0.01	0.26	0.23
CHILTON	0.74	0.77	0.72	0.99	0.82	0.84
SD	0.12	0.10	0.11	0.01	0.05	0.06
PRUHONICE	0.85	0.86	0.73	0.99	0.63	0.68
SD	0.11	0.07	0.17	0.01	0.13	0.11
ROME	0.84	0.83	0.83	0.99	0.84	0.84
SD	0.11	0.11	0.05	0.00	0.06	0.06
ATHENS	0.88	0.83	0.86	0.97	0.84	0.82
SD	0.07	0.10	0.03	0.02	0.06	0.06
EL ARENOSILLO	0.76	0.75	0.75	0.97	0.83	0.84
SD	0.12	0.15	0.08	0.02	0.10	0.05
AVERAGE	**0.79**	**0.79**	**0.74**	**0.98**	**0.74**	**0.75**
SD	**0.08**	**0.07**	**0.11**	**0.01**	**0.16**	**0.15**

On the other hand, during the solar maximum period, we observed even higher correlations for all source pairs (except the IRI–NeQuick pair), with values ranging from 0.86 to 0.90 and standard deviations within 0.10. This indicates a stronger overall consistency in TEC estimation among sources during periods of elevated solar activity.

Table 5: The average COR values at all locations and their respective average values in 2024

Location	$\overline{COR}_{ION-IRI}$	$\overline{COR}_{ION-NeQ}$	$\overline{COR}_{ION-GNSS}$	$\overline{COR}_{IRI-NeQ}$	$\overline{COR}_{IRI-GNSS}$	$\overline{COR}_{NeQ-GNSS}$
TROMSO	0.79	0.79	0.73	0.98	0.81	0.81
SD	0.09	0.10	0.29	0.03	0.17	0.16
CHILTON	/	/	/	0.99	0.87	0.87
SD	/	/	/	0.01	0.21	0.21
PRUHONICE	0.86	0.86	0.89	0.99	0.89	0.88
SD	0.18	0.18	0.13	0.01	0.15	0.16
ROME	/	/	/	0.99	0.93	0.94
SD	/	/	/	0.01	0.09	0.07
ATHENS	0.94	0.92	0.97	0.97	0.98	0.98
SD	0.03	0.05	0.02	0.03	0.01	0.01
EL ARENOSILLO	0.87	0.89	0.90	0.99	0.95	0.95
SD	0.20	0.14	0.12	0.02	0.05	0.05
AVERAGE	**0.87**	**0.86**	**0.87**	**0.98**	**0.90**	**0.90**
SD	**0.06**	**0.05**	**0.10**	**0.01**	**0.06**	**0.06**

Based on all created differences ΔTEC_{i-j_k}, we found the minimum (*MIN*) and maximum (*MAX*) values of all TEC differences ΔTEC_{i-j} for the years 2020, during the solar minimum period (Table 6), and 2024, during the solar maximum period (Table 7). The same tables also contain the averages (*AVG*) of the station averages for all TEC differences. Each station average is determined by the mean of the daily averages of ΔTEC_{i-j_k} for that specific station. We can see that each TEC source may produce TEC that differs from any other source by more than 9 TECU (except for $|\Delta TEC_{IRI-NeQ}|$ whose maximum is 6.5 TECU) within the solar minimum period. The solar maximum period demonstrates far greater differences over 30 TECU; still the differences between the IRI and NeQuick models reveal slightly lower values. It is worth noting that during selected days in the solar minimum phase, the TEC reaches maximum values exceeding 20 TECU, whereas in the solar maximum phase, TEC values exceed 70 TECU. In general, TEC during the solar maximum period was three to four times higher than during the solar minimum period.

Table 6: Values of statistical parameters MIN, MAX, and AVG for all TEC differences in 2020 given in TECU

Parameter	$\Delta TEC_{ION-IRI}$	$\Delta TEC_{ION-NeQ}$	$\Delta TEC_{ION-GNSS}$	$\Delta TEC_{IRI-NeQ}$	$\Delta TEC_{IRI-GNSS}$	$\Delta TEC_{NeQ-GNSS}$
MIN	-11.2	-10.0	-12.1	-4.7	-10.5	-9.1
MAX	7.6	8.1	5.1	6.5	7.3	7.9
AVG	-1.8	-2.4	-3.3	-0.8	-1.3	-0.4

Table 7: Values of statistical parameters MIN, MAX, and AVG for all TEC differences in 2024 given in TECU

Parameter	$\Delta TEC_{ION-IRI}$	$\Delta TEC_{ION-NeQ}$	$\Delta TEC_{ION-GNSS}$	$\Delta TEC_{IRI-NeQ}$	$\Delta TEC_{IRI-GNSS}$	$\Delta TEC_{NeQ-GNSS}$
MIN	-32.8	-45.3	-38.3	-23.3	-27.4	-15.6
MAX	27.4	17.6	13.3	12.1	19.2	35.7
AVG	-6.0	-8.1	-4.5	-4.1	-1.5	5.0

The averages analyzed during the solar minimum period indicate strong correlations between the TEC estimated by the NeQuick model and the TEC derived from GNSS data (below 0.5 TECU) as well as the TEC generated by the IRI model (below 1 TECU). During the same period, the IRI model produced TEC values that show a modest average difference from those derived from ionosondes and GNSS observations, ranging between 1 and 2 TECU. Larger absolute average differences are observed between the TEC obtained from ionosondes and that estimated by the NeQuick model (approximately 2.5 TECU), as well as between the TEC obtained from ionosondes and GNSS observations (greater than 3 TECU).

The average difference during the solar maximum phase consistently remained similar by itself between the TEC derived from the IRI model and GNSS data (around 1.5 TECU). The worst match at the solar maximum period is between TEC computed from ionosondes and the NeQuick model, with an average absolute value around 8 TECU. The remaining averages of TEC differences possess absolute values ranging from 4 to 6 TECU.

We computed daily *RMS* values for each location. Figure 3 shows the daily *RMS* results for the years 2020 and 2024, sourced from the same locations where we previously presented the TEC values. The daily *RMS* ranges between 0.4 TECU ($RMS_{ION–NeQ}$ several times) to 7.0 TECU ($RMS_{ION–GNSS}$ on 22/09/2020 at EL ARENOSILLO) during the solar minimum phase, and from 0.8 TECU ($RMS_{IRI–NeQ}$ on 20/06/2024 at TROMSO) to 27.2 TECU ($RMS_{ION–NeQ}$ on 11/05/2024 at EL ARENOSILLO) during the solar maximum phase. Certain tendencies associated with specific days in 2020 are not noticeable when examining daily *RMS* values. The *RMS* values obtained on different days within the solar minimum period at the same location are generally very similar.

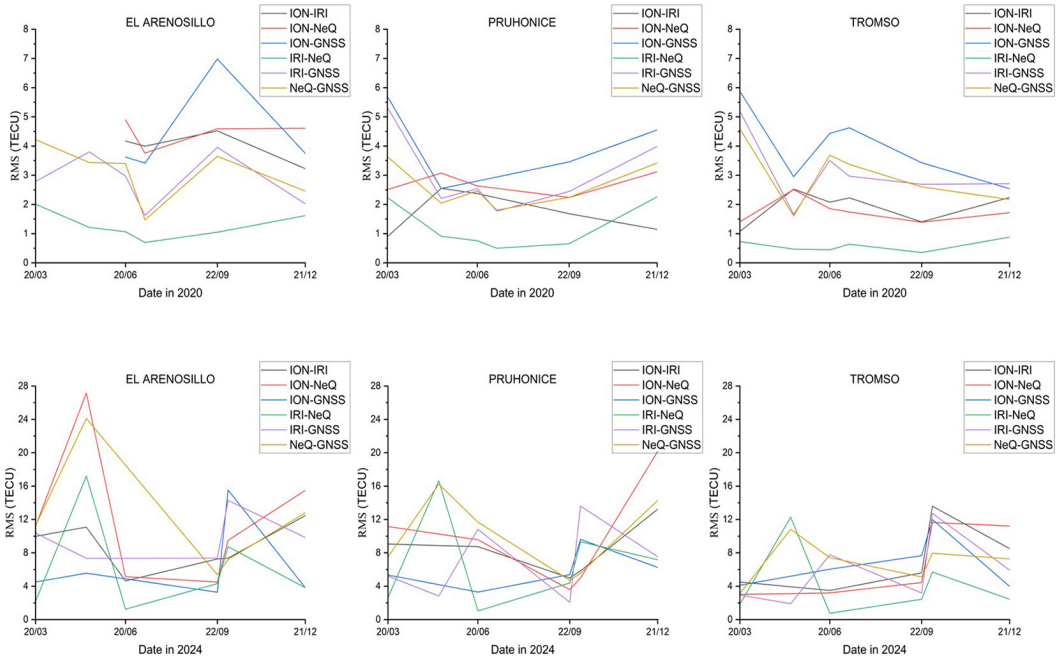

Figure 3: RMS values at locations TROMSO, PRUHONICE and EL ARENOSILLO during chosen days

Upon examining daily *RMS* values at the solar maximum period, we discovered some noteworthy findings. On the days 20/03/2024 and 22/09/2024, we noticed lower values for daily *RMS*s, indicating improved similarities between TEC. The specified days are characterized by decreased solar and geomagnetic activities. On 11/05/2024, during the time of extreme geomagnetic activity, the NeQuick model produced considerably higher TEC values; consequently, the daily RMS values, which account for TEC discrepancies involving the NeQuick model, were significantly higher on this day compared to others, with values two to three times greater. We also detected increasing $RMS_{ION–GNSS}$ values on a day that had extremely high solar activity (03/10/2024).

Using daily *RMS* values, we calculated their mean values and standard deviations for each location in 2020 (Table 8) and 2024 (Table 9). To ascertain consistency in daily *RMS* values at each location, we examined the obtained *SD* results. The analysis of the standard deviation of daily *RMS* results for the year 2020 revealed that it ranges from 0.2 to 1.7 TECU, with a mean value of 0.8 TECU. Considering this, we ascertained that daily *RMS* values are very consistent in the solar minimum period. It means that TEC differences during the solar minimum period are uniform over selected days at particular locations. The most consistent daily *RMS*s is $RMS_{ION–NeQ}$ with an average *SD* of 0.5 TECU, as well as $RMS_{ION–IRI}$ and $RMS_{IRI–NeQ}$ with an average *SD* of 0.6 TECU. The biggest average *SD* is for $RMS_{ION–GNSS}$ (1.4 TECU). The standard deviations for the remaining *RMS*s average around 1 TECU. We noted that the TEC derived from GNSS data demonstrated the lowest consistency during the solar minimum period.

On the other hand, the solar maximum period demonstrated drastically lower consistency in daily *RMS* values. The examination of the standard deviation of daily *RMS* results for 2024 showed a range of 1.1 to 8.4 TECU, with a mean value of 4.3 TECU, approximately five times larger than the values obtained in 2020. Acceptable consistency was shown by $RMS_{ION–IRI}$, $RMS_{ION–GNSS}$, and $RMS_{IRI–GNSS}$ with an average *SD* below 3.5 TECU. The average *SD* values for the remaining *RMS* values ranged from 4.5 to 6 TECU, indicating substantial inconsistency in the TEC produced by the NeQuick model through the solar maximum phase. These results, particularly those from the solar minimum period, encouraged the computation and analysis of stations' $\overline{RMS}_{i–j}$.

Alongside the stations' averages ($\overline{RMS}_{i–j}$), Table 8 and Table 9 also present the overall averages for each TEC difference, calculated as the mean of the stations' averages, as well as corresponding standard deviations. Upon analyzing the obtained standard deviations, it is evident that the station's $\overline{RMS}_{i–j}$ values showed excellent consistency during the solar minimum phase (range 0.3 to 1.0 TECU) and quite satisfactory consistency during the solar maximum phase (range 1.1 to 3.1 TECU), enabling the generation of conclusions based on the means of stations' averages.

Table 8: The average RMS values at all locations and their respective average values in 2020 given in TECU

Location	$\overline{RMS}_{IOM–IRI}$	$\overline{RMS}_{IOM–NeQ}$	$\overline{RMS}_{IOM–GNSS}$	$\overline{RMS}_{IRI–NeQ}$	$\overline{RMS}_{IRI–GNSS}$	$\overline{RMS}_{NeQ–GNSS}$
TROMSO	1.9	1.8	4.0	0.6	3.1	3.0
SD	0.6	0.4	1.2	0.2	1.2	1.1
CHILTON	2.0	2.6	3.1	0.9	2.1	2.3
SD	0.6	0.3	1.7	0.6	1.1	0.9
PRUHONICE	1.7	2.7	3.8	1.2	3.0	2.6
SD	0.7	0.4	1.3	0.8	1.3	0.8

Location	$\overline{RMS}_{IOM-IRI}$	$\overline{RMS}_{IOM-NeQ}$	$\overline{RMS}_{IOM-GNSS}$	$\overline{RMS}_{IRI-NeQ}$	$\overline{RMS}_{IRI-GNSS}$	$\overline{RMS}_{NeQ-GNSS}$
ROME	2.8	3.5	4.1	1.5	2.5	2.4
SD	0.8	1.1	1.2	0.7	0.9	0.3
ATHENS	3.0	4.3	4.3	1.7	2.6	2.5
SD	0.6	0.3	1.3	0.7	1.0	0.6
EL ARENOSILLO	4.0	4.5	4.4	1.3	2.9	3.1
SD	0.5	0.5	1.7	0.5	0.9	1.0
AVERAGE	**2.6**	**3.2**	**4.0**	**1.2**	**2.7**	**2.7**
SD	0.9	1.0	0.5	0.4	0.4	0.3

Table 9: The average RMS values at all locations and their respective average values in 2024 given in TECU

Location	$\overline{RMS}_{IOM-IRI}$	$\overline{RMS}_{IOM-NeQ}$	$\overline{RMS}_{IOM-GNSS}$	$\overline{RMS}_{IRI-NeQ}$	$\overline{RMS}_{IRI-GNSS}$	$\overline{RMS}_{NeQ-GNSS}$
TROMSO	7.1	6.7	6.8	4.2	5.7	6.9
SD	4.1	4.4	3.3	4.3	4.1	2.6
CHILTON	/	/	/	6.7	7.3	9.8
SD	/	/	/	5.6	4.0	3.0
PRUHONICE	8.4	9.9	6.0	6.9	7.0	10.0
SD	3.2	6.5	2.3	5.7	4.5	4.8
ROME	/	/	/	6.9	6.4	9.6
SD	/	/	/	5.5	3.1	5.3
ATHENS	11.7	13.7	9.9	7.4	7.1	7.7
SD	3.2	4.1	3.1	5.2	1.1	2.6
EL ARENOSILLO	8.8	12.2	6.5	6.2	9.8	12.2
SD	2.9	8.4	5.1	6.0	2.8	7.3
AVERAGE	9.0	10.6	7.3	6.4	7.2	9.4
SD	1.9	3.1	1.8	1.1	1.4	1.8

During the solar minimum period, the $\overline{RMS}_{ION-IRI}$ and $\overline{RMS}_{ION-NeQ}$ showed a slightly lower consistency with *SD* around 1 TECU, whereas the other SD values remained below 0.5 TECU. During the solar maximum period, the scenario was similar, with $\overline{RMS}_{ION-NeQ}$ exhibiting the lowest consistency, showing an *SD* of 3.1 TECU. The most consistent was $\overline{RMS}_{IRI-NeQ}$, exhibiting an *SD* of 1.1 TECU. Subsequently, we identified $\overline{RMS}_{IRI-GNSS}$ having a standard deviation of 1.4 TECU, while the remaining $\overline{RMS}_{i-j}$ values showed standard deviation values close to 2 TECU. Although the $\overline{RMS}_{i-j}$ values at all stations remained relatively stable, we observed that at TROMSO, the northernmost location in our study, the TEC values from different sources were noticeably more consistent. This trend was particularly evident during the solar maximum period, where all $\overline{RMS}_{i-j}$ values at TROMSO were approximately 25% lower than at other locations. During the solar minimum period, $\overline{RMS}_{i-j}$ values at TROMSO also tended to be lower, with the exception of the $\overline{RMS}_{i-j}$ corresponding to TEC derived from GNSS. However, it is important to note that the TEC values themselves were also lower at TROMSO compared to other locations, particularly in contrast to ATHENS and EL ARENOSILLO, which are the southernmost stations in our dataset. Due to the homogeneity of the station's $\overline{RMS}_{i-j}$, we will draw conclusions based on their averages to ascertain the magnitude of TEC differences.

First, it is noticeable that the average $\overline{RMS}_{i-j}$ values (Table 8 and Table 9) correspond to the absolute values of the overall *AVG* (Table 6 and Table 7) and exhibit some resemblance. This indicates a systematic bias in the TEC values derived from different sources. The diagrams presented in Figure 2 already demonstrated this (generally, TEC from ionosondes is the smallest, TEC from GNSS or the NeQuick model is the largest, and so on).

We separately analyzed $\overline{RMS}_{i-j}$ values for the solar minimum and solar maximum periods due to the clear differences in the obtained values. Studying the computed $\overline{RMS}_{i-j}$ values in the solar minimum period, we found that they range from 1.2 to 4.0 TECU, leading us to the following outcomes:

- The IRI and NeQuick models produced TEC that were highly consistent with each other, with an RMS value of 1.2 TECU.
- The second-best correspondence is noticed between the TEC obtained from ionosondes and that derived from the IRI model, with an RMS value slightly above 2.5 TECU. Similar discrepancies occurred between the TEC obtained from GNSS data and the TEC produced by the NeQuick and IRI models.
- TEC derived from ionosondes and the NeQuick model had larger differences, quantified at 3.2 TECU.
- The largest discrepancies (4.0 TECU) arose from the TEC obtained from ionosondes and GNSS data.

Upon studying the computed $\overline{RMS}_{i-j}$ values during the solar maximum period, we found that they range between 6.4 and 10.6 TECU, leading us to the following findings:

- The best correspondence between the TEC obtained from the IRI and NeQuick models was noticed (6.4 TECU).
- We found the second-highest similarity (7.2 TECU) between TEC obtained from the IRI model and GNSS measurements. TEC derived from GNSS observations showed similar correspondence with TEC obtained from ionosondes (7.3 TECU).
- TEC derived from ionosondes and the IRI model had an *RMS* value of 9.0 TECU, while TEC obtained from GNSS data and the NeQuick model showed a somewhat worse correspondence with an RMS value of 9.4 TECU.
- The worst correspondence was between TEC obtained from ionosondes and the NeQuick model.

6 CONCLUSION

We reached certain conclusions upon analyzing TEC values from six European locations obtained from ionosondes, the IRI model, the NeQuick model, and GNSS measurements. In general, ionosondes yield the lowest TEC results during both the solar minimum and solar maximum phases. During periods of low solar and geomagnetic activity, GNSS data produce the highest TEC values; whereas, under conditions of strong solar and geomagnetic activity, the NeQuick model generates the highest TEC values. The TEC calculated using the NeQuick model markedly increases with geomagnetic activity. The IRI model typically produces TEC values comparable to those of the NeQuick model, especially during periods of low solar and geomagnetic activity.

Analyzing temporal changes, we found that the diurnal variations in TEC from different sources exhibit significant similarity, achieving a daily correlation coefficient beyond 0.74 during the solar minimum

period and 0.86 during the solar maximum period. At the northernmost station in our dataset, decreased correlations appeared under low solar activity conditions.

We discovered that several TEC sources produce TEC with a satisfactory level of consistency across Europe. The consistency level of various TEC sources is around several TECU at solar minimum and within 10 TECU during solar maximum. The average ratio of overall RMS values at solar maximum and solar minimum periods is approximately 3.5 TECU, in line with their standard deviations. This relationship is similar to the correspondence between TEC values during solar maximum and minimum periods, wherein the solar maximum phase yields three to four times greater TEC than the solar minimum phase, resulting in an equivalent ratio of the highest TEC values at solar maximum (71.24 TECU) and minimum (22.2 TECU) phases.

The IRI and NeQuick models produce TEC that are highly consistent with each other at both the solar minimum (RMS of 1.2 TECU) and solar maximum (RMS of 6.4 TECU) phases. During the solar minimum period, the inconsistencies between the TEC values calculated from GNSS measurements and those from the NeQuick and IRI models are very small, with RMS values slightly above 2.5 TECU. Ionosondes exhibit identical consistency in TEC with the IRI model; however, larger discrepancies occur with TEC obtained from the NeQuick model (3.2 TECU) and GNSS data (4.0 TECU) during the solar minimum phase. During the solar maximum period, GNSS observations provide TEC that aligns more closely with TEC obtained from the IRI model and ionosondes (RMS around 7 TECU) than with TEC produced by the NeQuick model (RMS of 9.4 TECU). TEC obtained from ionosondes and the IRI model have large discrepancies (RMS of 9.0 TECU), but the largest ones are between TEC derived from ionosondes and the NeQuick model, with an RMS above 10 TECU. TROMSO, the northernmost location in our research, showed smaller differences (around 25% lower RMS values) between TEC than other locations, while simultaneously exhibiting lower TEC values generally compared to other locations.

This study encompassed a comparative analysis of TEC values obtained from various sources during two distinct phases of solar activity: six days in 2020 representing the solar minimum and six days in 2024 corresponding to the solar maximum. Although the selected days provided valuable insight into the consistency of TEC values obtained from various sources (ionosondes, GNSS, the IRI model, and the NeQuick model), further research covering a broader temporal span across multiple years, particularly during periods of intriguing solar and geomagnetic activity, could further improve the reliability of these comparisons. Based on the obtained results, we believe that conducting a detailed examination of the TEC values generated by the NeQuick model during periods of intense geomagnetic activity would be noteworthy. The results presented in this study were obtained by calculating TEC at six locations evenly distributed across Europe, with station latitudes ranging from 35°N to 70°N. The results warrant further examination over different latitudes, especially at equatorial and low-latitude regions. Furthermore, studies need to be carried out in the Southern Hemisphere to provide further valuable insight.

Literature and references:

Ameen, M. A., Jabbar, M. A., YU, X., Zhen, W., Murtaza, G., Chishtie, F., Khursheed, H., Atiq, M. (2019). Comparison of Ionospheric Total Electron Content (TEC)

over Sonmiani (Pakistan) with NeQuick-2 and IRI-2012 during July 2014 – June 2015. Advances in Space Research, 63(6), 1882–1891. DOI: https://doi.org/10.1016/j.asr.2018.09.017.

Atıcı, R. (2018). Comparison of GPS TEC with modelled values from IRI 2016 and IRI-PLAS over Istanbul, Turkey. Astrophysics and Space Science, 363(11), 231. DOI: https://doi.org/10.1007/s10509-018-3457-0.

Bilitza, D. (1990). International Reference Ionosphere 1990. National Space Science Data Center, Report 90-22. Retrieved from https://irimodel.org/docs/IRI1990pp0-84.pdf.

Bilitza, D., Pezzopane, M., Truhlik, V., Altadill, D., Reinisch, B. W., Pignalberi, A. (2022). The International Reference Ionosphere Model: A Review and Description of an Ionospheric Benchmark. Reviews of Geophysics, 60(4). DOI: https://doi.org/10.1029/2022RG000792.

Chen, J., Ren, X., Zhang, X., Zhang, J., Huang, L. (2020). Assessment and Validation of Three Ionospheric Models (IRI-2016, NeQuick2, and IGS-GIM) From 2002 to 2018. Space Weather, 18(6). DOI: https://doi.org/10.1029/2019SW002422.

Ciraolo, L., Azpilicueta, F., Brunini, C., Meza, A., Radicella, S. M. (2007). Calibration errors on experimental slant total electron content (TEC) determined with GPS. Journal of Geodesy, 81(2), 111–120. DOI: https://doi.org/10.1007/s00190-006-0093-1.

Cooper, C., Mitchell, C. N., Wright, C. J., Jackson, D. R., Witvliet, B. A. (2019). Measurement of Ionospheric Total Electron Content Using Single-Frequency Geostationary Satellite Observations. Radio Science, 54(1), 10–19. DOI: https://doi.org/10.1029/2018RS006575.

Dach, R., Lutz, S., Walser, P., Fridez, P. (Eds.). (2015). Bernese GNSS Software Version 5.2 (User manual). Astronomical Institute, University of Bern, Bern Open Publishing. DOI: https://doi.org/10.7892/boris.72297.

Davies, K. (1990). Ionospheric Radio. Institution of Engineering and Technology. DOI: https://doi.org/10.1049/PBEW031E.

Foelsche, U., Kirchengast, G. (2002). A simple "geometric" mapping function for the hydrostatic delay at radio frequencies and assessment of its performance. Geophysical Research Letters, 29(10). DOI: https://doi.org/10.1029/2001GL013744.

Galkin, I. A., Reinisch, B. W. (2011). Global Ionospheric Radio Observatory (GIRO): Status and prospective. 2011 XXXth URSI General Assembly and Scientific Symposium, 1–4. DOI: https://doi.org/10.1109/URSIGASS.2011.6050896.

Guo, Z., Yao, Y., Kong, J., Chen, G., Zhou, C., Zhang, Q., Shan, L., Liu, C. (2021). Accuracy Analysis of International Reference Ionosphere 2016 and NeQuick2 in the Antarctic. Sensors, 21(4), 1551. DOI: https://doi.org/10.3390/s21041551.

Hargreaves, J. K. (1992). The Solar-Terrestrial Environment. Cambridge University Press. DOI: https://doi.org/10.1017/CBO9780511628924.

Hernández-Pajares, M., Juan, J. M., Sanz, J., Orus, R., Garcia-Rigo, A., Feltens, J., Komjathy, A., Schaer, S. C., Krankowski, A. (2009). The IGS VTEC maps: a reliable source of ionospheric information since 1998. Journal of Geodesy, 83(3–4), 263–275. DOI: https://doi.org/10.1007/s00190-008-0266-1.

Hofmann-Wellenhof, B., Lichtenegger, H., Wasle, E. (2008). GNSS — Global Navigation Satellite Systems. Springer Vienna. DOI: https://doi.org/10.1007/978-3-211-73017-1.

Hoque, M. M., Jakowski, N. (2008). Estimate of higher order ionospheric errors in GNSS positioning. Radio Science, 43(5). DOI: https://doi.org/10.1029/2007RS003817.

Kayode, Y. O., Okoh, D., Onori, E. O., Ometan, O. O., Adegbola, R. B., Ogwala, A., Somoye, E. O., Adeniji-Adele, R. A. (2024). Effects of local time on the variations of the total electron contents at an American and Asian longitudes and their comparison with IRI-2016, IRI-Plas2017 and NeQuick-2 models during solar cycle 24. Journal of Atmospheric and Solar-Terrestrial Physics, 260, 106271. DOI: https://doi.org/10.1016/j.jastp.2024.106271.

Klipp, T. dos S., Petry, A., de Souza, J. R., de Paula, E. R., Falcão, G. S., de Campos Velho, H. F. (2020). Ionosonde total electron content evaluation using International Global Navigation Satellite System Service data. Annales Geophysicae, 38(2), 347–357. DOI: https://doi.org/10.5194/angeo-38-347-2020.

Klobuchar, J. (1987). Ionospheric Time-Delay Algorithm for Single-Frequency GPS Users. IEEE Transactions on Aerospace and Electronic Systems, AES-23(3), 325–331. DOI: https://doi.org/10.1109/TAES.1987.310829.

Klobuchar, J. A. (1991). Ionospheric Effects on GPS. GPS World, 2, 48–51.

Matzka, J., Stolle, C., Yamazaki, Y., Bronkalla, O., Morschhauser, A. (2021). The Geomagnetic Kp Index and Derived Indices of Geomagnetic Activity. Space Weather, 19(5). DOI: https://doi.org/10.1029/2020SW002641.

Memarzadeh, Y. (2009). Ionospheric Modeling for Precise GNSS Applications. Delft University of Technology.

Mood, A., Graybill, F., Boes, D. (1974). Introduction to the Theory of Statistics (3rd ed.). McGraw-Hill.

Nava, B., Coïsson, P., Radicella, S. M. (2008). A new version of the NeQuick ionosphere electron density model. Journal of Atmospheric and Solar-Terrestrial Physics, 70(15), 1856–1862. DOI: https://doi.org/10.1016/j.jastp.2008.01.015.

Odeyemi, O. O., Adeniyi, J., Oladipo, O., Olawepo, O., Adimula, I., Oyeyemi, E. (2018). Morphology of GPS and DPS TEC over an equatorial station: validation of IRI and NeQuick 2 models. Annales Geophysicae, 36(5), 1457–1469. DOI: https://doi.org/10.5194/angeo-36-1457-2018.

Reinisch, B. W., Galkin, I. A. (2011). Global Ionospheric Radio Observatory (GIRO). Earth, Planets and Space, 63(4), 377–381. DOI: https://doi.org/10.5047/eps.2011.03.001.

Sardón, E., Rius, A., Zarraoa, N. (1994). Estimation of the transmitter and receiver differential biases and the ionospheric total electron content from Global Positioning System observations. Radio Science, 29(3), 577–586. DOI: https://doi.org/10.1029/94RS00449.

Schaer, S. (1999). Mapping and Predicting the Earth's Ionosphere Using the Global Positioning System. University of Berne.

Schunk, R. W., Nagy, Andrew. (2009). Ionospheres: physics, plasma physics, and chemistry. Cambridge University Press.

Seemala, G. K. (2023). Estimation of ionospheric total electron content (TEC) from GNSS observations. In Atmospheric Remote Sensing (pp. 63–84). Elsevier. DOI: https://doi.org/10.1016/B978-0-323-99262-6.00022-5.

Todorović Drakul, M., Grekulović, S., Odalović, O., Petković, D. (2021). Comparison of IRI-2016 and NeQuick models of the ionosphere over the Balkan Peninsula during the year 2019. Contemporary Theory and Practice in Construction, 15(1). DOI: https://doi.org/10.7251/stp2215283t.

Wilks, D. (2006). Statistical Methods in the Atmospheric Science (2nd ed.). Academic Press.

Wu, M., Guo, P., Zhou, W., Xue, J., Han, X., Meng, Y., Hu, X. (2021). A New Mapping Function for Spaceborne TEC Conversion Based on the Plasmaspheric Scale Height. Remote Sensing, 13(23), 4758. DOI: https://doi.org/10.3390/rs13234758.

Xiang, Y., Gao, Y. (2019). An Enhanced Mapping Function with Ionospheric Varying Height. Remote Sensing, 11(12), 1497. DOI: https://doi.org/10.3390/rs11121497.

Xu, W., Marshall, R. A., Bortnik, J., Bonnell, J. W. (2021). An Electron Density Model of the D- and E-Region Ionosphere for Transionospheric VLF Propagation. Journal of Geophysical Research: Space Physics, 126(7). DOI: https://doi.org/10.1029/2021JA029288.

Yasyukevich, Y. V., Zatolokin, D., Padokhin, A., Wang, N., Nava, B., Li, Z., Yuan, Y., Yasyukevich, A., Chen, C., Vesnin, A. (2023). Klobuchar, NeQuickG, BDGIM, GLONASS, IRI-2016, IRI-2012, IRI-Plas, NeQuick2, and GEMTEC Ionospheric Models: A Comparison in Total Electron Content and Positioning Domains. Sensors, 23(10), 4773. DOI: https://doi.org/10.3390/s23104773.

Krstić S., Todorović-Drakul M., Grekulović S., Petković D., Odalović O. (2025). Comparison of Total Electron Content Sources Over Europe During Solar Minimum and Maximum Years (2020 and 2024). Geodetski vestnik, 69 (4), 574-593.
DOI: https://doi.org/10.15292/geodetski-vestnik.2025.04.574-593

Stefan Krstić, Ph.D. Candidate
University of Belgrade, Faculty of Civil Engineering
Bulevar kralja Aleksandra 73, 11000 Belgrade, Serbia
e-mail: skrstic@grf.bg.ac.rs

Miljana Todorović-Drakul, Ph.D.
University of Belgrade, Faculty of Civil Engineering
Bulevar kralja Aleksandra 73, 11000 Belgrade, Serbia
e-mail: mtodorovic@grf.bg.ac.rs

Sanja Grekulović, Ph.D.
University of Belgrade, Faculty of Civil Engineering
Bulevar kralja Aleksandra 73, 11000 Belgrade, Serbia
e-mail: sanjag@grf.bg.ac.rs

Dušan Petković, Ph.D.
University of Belgrade, Faculty of Civil Engineering
Bulevar kralja Aleksandra 73, 11000 Belgrade, Serbia
e-mail: dpetkovic@grf.bg.ac.rs

Oleg Odalović, Ph.D.
University of Belgrade, Faculty of Civil Engineering
Bulevar kralja Aleksandra 73, 11000 Belgrade, Serbia
e-mail: odalovic@grf.bg.ac.rs